PHYSICAL REVIEW D VOLUME 22, NUMBER 11 1 DECEMBER 1980

Total and partial $\bar{p}d$ cross sections from 0.26 to 0.47 GeV/c

T. Kalogeropoulos and G. S. Tzanakos
Physics Department, Syracuse University, Syracuse, New York 13210
(Received 28 November 1979; revised manuscript received 9 April 1980)

The $\bar{p}d$ total cross section is $\sim 10\%$ larger than the $A + B/P$ extrapolated cross section seen at higher (~ 0.5–2.0 GeV/c) momenta. The excess is mainly due to the nonannihilation part of the total cross section. The $\bar{p}p$ annihilation cross sections in H_2 and D_2 are the same. These observations are consistent with known properties of the $\bar{N}N(1897)$. A 3σ dip is present at ~ 0.43 GeV/c mainly due to $p\bar{p}$ annihilation. This dip cannot be understood in terms of a single resonance at $\bar{N}N(1897)$ and the $S(1935)$. Our cross sections are ~ 10–20% higher than the recent measurements of Hamilton *et al.*

I. INTRODUCTION

Interest in $\bar{N}N$ interactions near threshold has increased in recent years as a result of observations and theoretical considerations. The extensive studies at rest produced many puzzling phenomena that could be interpreted in terms of narrow states[1] while the in-flight studies yielded evidence[2-5] for two states: $S(1935)$ and $\bar{N}N(1897)$. On the theoretical side, potential[6] and constituent[7] models predict many $\bar{N}N$ states near threshold. We have completed the analysis of a bubble-chamber experiment in which the $\bar{p}d$ cross sections have been measured near threshold where present data are scarce.

The $S(1935)$ was considered as an established state up to recently. It has been seen[2,4,5] in $\bar{p}p$ and $\bar{p}d$ cross sections. The $\bar{N}N(1897)$ has been seen[3] in a study of the missing-mass spectra $\bar{p}d \to p_s + (\mathrm{MM})^-$. [The $S(1935)$ has also been seen in Ref. 3 but with far less statistical significance than the $\bar{N}N(1897)$.] The production of the $\bar{N}N(1897)$ is sensitive to spectator momentum. It is produced in association with "spectators" of momenta $\gtrsim 0.175$ GeV/c and the production is maximum at ~ 0.25 GeV/c.

An important question regarding the nature of the $\bar{N}N(1897)$ bump is whether it might be a reflection of elastic $\bar{p}p$ scattering followed by $\bar{p}n$ annihilation. The sharp dependence of its production on spectator momentum has been used as an argument against this interpretation. On the other hand, since the elastic and annihilation cross sections vary smoothly with energy, this two-step mechanism should contribute smoothly at all energies and therefore it should not manifest itself as an enhancement in the total $\bar{p}d$ cross section. In this paper evidence is presented of such an enhancement which lends independent support to the conclusion drawn in Ref. 3, namely, that the $\bar{N}N(1897)$ bump is the result of a direct $\bar{p}n$ interaction.

II. ANALYSIS

The $\bar{p}d$ cross sections were measured by analyzing interactions of a pure $\bar{p}$ beam brought to rest at the downstream end of the BNL 30-in. bubble chamber. Thus, we were able to study $\bar{p}d$ interactions in flight and at rest in a continuous manner and avoid point-to-point systematic errors. Each antiproton entering the chamber (~ 5/picture) was measured up to the interaction vertex and the topology was recorded. The measurements were taken on line to a computer and among other things the smoothness of beam tracks was being continuously checked and small-angle scatters detected. All measured events (~31 000) were processed by the standard bubble-chamber reconstruction program TVGP (three-view-geometry program) which was developed at the Lawrence Radiation Laboratory. The TVGP output was compared with the film information on the scanning table. Missing or misidentified events were remeasured and thus an overall efficiency of 98.5% was achieved.

Correct determination of momentum, avoiding contamination by at-rest annihilations, and flux dependence on momentum have been prime concerns of this work. Although the details are given in Ref. 8, for completeness, some important tests will be presented.

The momentum has been obtained by properly weighting (according to errors) the momentum determined from the curvature of the tracks (P_C) and the momentum obtained from residual range (P_R). The residual range is defined as the difference between the track length and the mean range. The error on P_C is calculated in TVGP which takes into account quality of the fit and Coulomb scattering. This error δP_C has been found to agree on the average with $(P_C - P_R)/P_R$ for stopping protons. The error on P_R has been evaluated from the uncertainty (~±4 cm) in range. P_R has been calibrated with μ^+ from π^+ decays (Fig. 1), and

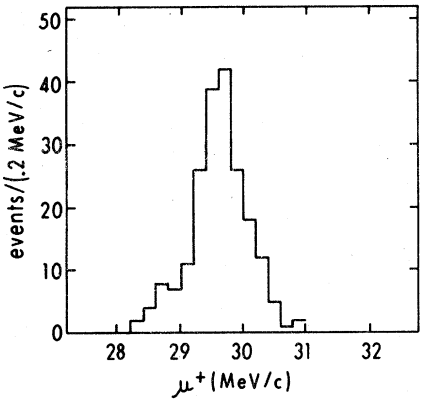

FIG. 1. Momentum distribution of stopping μ^+ coming from π^+ (stopping) decays. The average μ^+ momentum measured is (29.81 ± 0.03) MeV/c which is in excellent agreement with 29.80 MeV/c expected from the π^+, μ^+, ν masses.

P_C with stopping protons (Fig. 2). Furthermore, in a study of $\bar{p}d \to \bar{p}'d'$, in which $\bar{p}'$ and d' stop, we found excellent momentum balance between $\bar{p}$ and $\bar{p}' + d'$.

We have studied stopping distrubtions as a function of entrance variables and found a smooth dependence (Fig. 3) of the beam momentum on entrance point, and a sharp break probably due to a misplaced beam counter in front of the chamber window, producing two beam components (Fig. 4), in this exposure. We determined cross sections for both "beams" and the results are in excellent agreement (Fig. 5). The contamination of the in-flight events by at-rest annihilations has been studied as follows. First, we estimated the fraction of in-flight annihilations in the stopping region (<10 cm) to be 0.20 ± 0.01. This was done

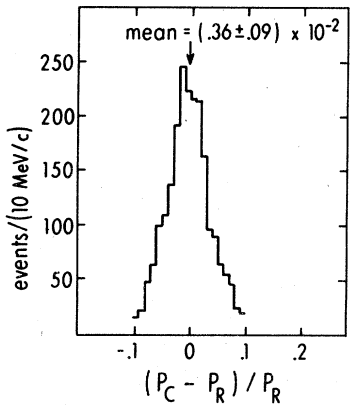

FIG. 2. Comparison of momenta by curvature (P_C) and range (P_R) for stopping protons of length >20 cm. P_C is possibly underestimated by negligible amount (~0.36%).

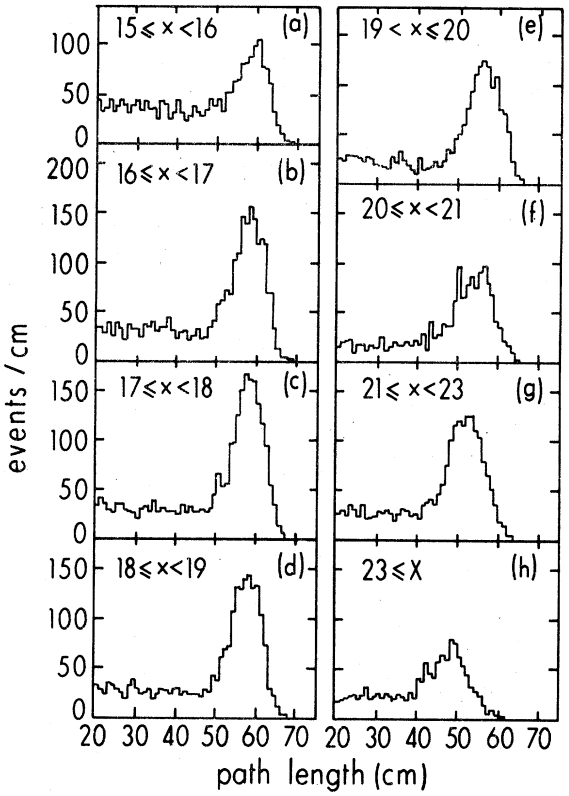

FIG. 3. Typical stopping distributions as a function of the entrance coordinate. The widths of the stopping distributions are ~±4 cm.

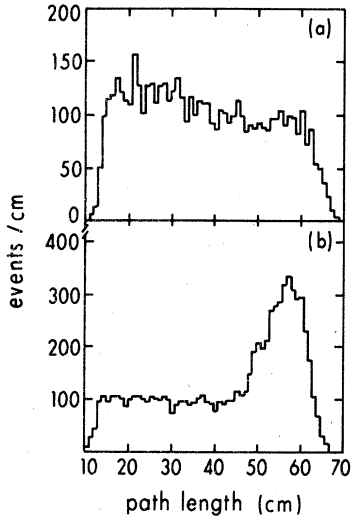

FIG. 4. Vertex distributions along the beam for the two beam components identified by entrance coordinate. One of the beams exits the chamber (a) while the other is stopping (b).

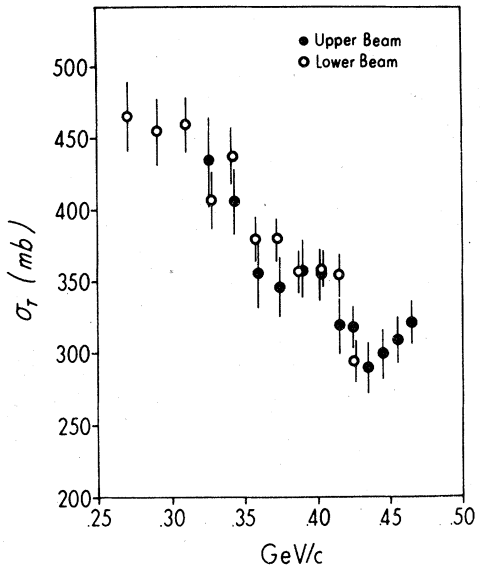

FIG. 5. The $\bar{p}d$ total cross section as found independently from the two beam components.

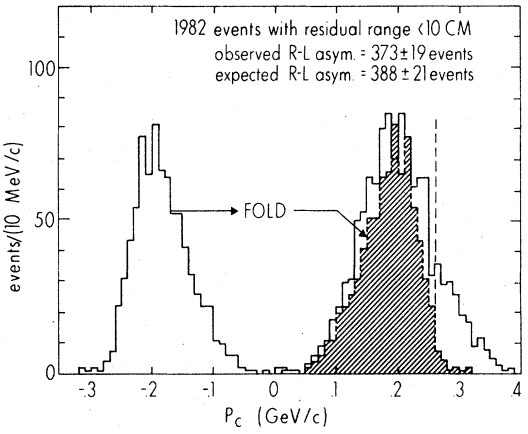

FIG. 7. The selection of in-flight annihilations in the stopping region based on the vertex momentum (P_C) which was evaluated from the curvature at the middle of the track. The asymmetry around $P_C = 0$ is due to in-flight annihilations. By folding the region $P_C < 0$ into $P_C > 0$, one can see that events with $P_C \gtrsim 0.26$ GeV/c are in-flight. (See details in text.)

by computing the shape of their distribution and matching it with the in-flight distribution outside the stopping region. Figure 6 shows the resulting in-flight and at-rest distributions as well as the distribution of elastic events for comparison. Subsequently we attempted to separate in-flight from at-rest annihilations in the stopping region on an event-by-event basis. For these events the beam traverses almost the entire chamber and the curvature is well measured. TVGP computes curvature, momentum, and corresponding range at the middle of each track. Then it swims the track to the vertex, subtracts the traversed length to make residual range, and from this it computes the momentum (P_C) at the vertex (Fig. 7). For a symmetric at-rest distribution of particles (like the one of Fig. 6) the resulting P_C distribution is expected to be symmetric (see also Fig. 2 for stopping protons). In-flight events will show as an excess in the region of positive P_C. (Negative P_C means that the momentum at the middle of the track is underestimated. The zero in the center is implied by the transformation of residual range into momentum: $dR \propto p^{2.5} dp$). The observed R-L asymmetry corresponds to a fraction 0.19 ± 0.01 in very good agreement with the earlier computed estimate of 0.20 ± 0.01. Clearly, the in-flight events dominate above 0.26 GeV/c. Notice that the contamination seen in Fig. 7 is an overestimate since most

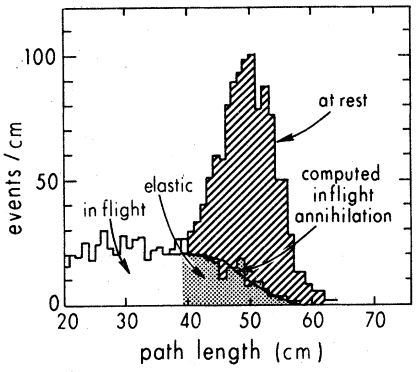

FIG. 6. $\bar{p}$ path-length distribution for annihilation and elastic events in D_2. The number of elastic events is scaled so that the two distributions match in the in-flight region. The in-flight distribution in the stopping region, computed from the annihilation events, is in very good agreement with the distribution of elastic events.

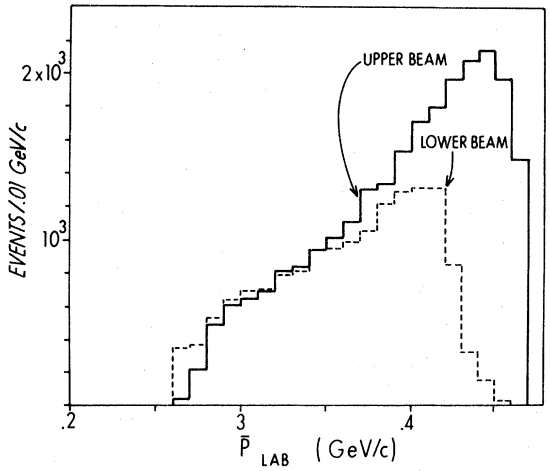

FIG. 8. Events measured as a function of antiproton momentum and used for the determination of cross sections.

TABLE I. Annihilation branching ratios in deuterium. Each column has been normalized to 100. (See Table II for $\bar{p}n/\bar{p}p$ ratios.)

Charged multiplicity	$\bar{p}p$ Rest	$\bar{p}p$ Flight	$\bar{p}n$ Rest	$\bar{p}n$ Flight
0	6.4±0.4	5.5±2[a]		
1			16.8±0.8	18.4±0.8
2	42.3±1.0	39.7±1.0		
3			59.5±1.4	59.5±1.4
4	46.9±1.1	50.0±1.1		
5			23.0±0.9	21.7±0.9
6	4.4±0.3	4.8±0.3		
7			0.7±0.2	0.4±0.1
Total	100.0	100.00	100.0	100.0

[a] Zero-prong events account for (14.6±0.6)% of the annihilation in flight. The charge-exchange contribution was estimated from associated n stars and has been subtracted.

of our in-flight events do not come from the stopping region. To summarize, (a) all events with $P_C < 0.26$ GeV/c are considered to be at rest, (b) the momentum assignment at the interaction vertex is (P_C) for in-flight events in the stopping region (<10 cm) and a weighted average of (P_C) and (P_R) for events in the in-flight region.

Every antiproton entering the chamber has been measured up to the end of its range and the flux is thus determined simply from the measurements. Figure 8 shows the distributions of interacting antiprotons as a function of vertex momenta. We have calculated cross sections throughout the momentum range shown in Fig. 8. The cross sections extrapolate smoothly in the region of rapid flux changes.

Based on these tests and procedures, we are confident that (a) the $\bar{p}$ momentum is measured well, (b) the at-rest contamination above 0.3 GeV/c is negligible, (c) the deuterium density is correct, (d) the flux is well known, and (e) apart from small-angle scatters, the efficiency for identifying interactions is better than 98%.

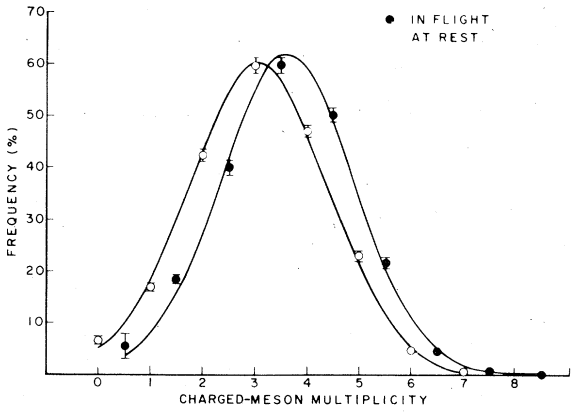

FIG. 9. Annihilation branching ratios in deuterium. For clarity, the in-flight data have been displaced horizontally by half a unit. The $(\bar{p}n)$ (odd number of charged mesons) and $(\bar{p}p)$ frequencies have been normalized to one independently. The curves are Gaussians with fitted parameters (mean, standard deviation) = (3.05±0.02, 1.35±0.01) at rest, (3.11±0.02, 1.29±0.01) in-flight.

III. RESULTS

(a) The branching ratios for $\bar{p}p$ and $\bar{p}n$ annihilations obtained in this experiment are presented in Table I. The branching ratios for $\bar{p}p$ at rest are in very good agreement with those observed[9] in H_2 apart from the zero-prong topology. In H_2 this branching ratio was reported as (3.2±0.5)%. The $\bar{p}p$ and $\bar{p}n$ branching ratios, normalized separately, fit very well to Gaussians (Fig. 9) with means $\langle N_\pm \rangle$ and standard deviations $\delta N_\pm$ given in Table II. (Gaussians have been used in a statistical bootstrap model[10] which has been very successful in describing annihilation branching ratios.) The ratio of annihilation on neutrons to protons, $\bar{p}n/\bar{p}p$, is significantly smaller than one (see Table II). The larger error for in-flight events is a reflection of the uncertainty in charge exchange. If Γ_0, Γ_1 are the total widths for annihilation from $I=0,1$ states, then

$$\bar{p}n/\bar{p}p = 2\Gamma_1/(\Gamma_0+\Gamma_1) \qquad (1)$$

from which the Γ_1/Γ_0 ratios are extracted (see

TABLE II. Comparison of $\bar{p}n$, $\bar{p}p$ annihilations in deuterium at rest and in flight. (See text.)

	Rest	Flight
$\bar{p}n/\bar{p}p$	0.749±0.018	0.863±0.033
Γ_1/Γ_0	0.598±0.023	0.759±0.089
$\langle N_\pm \rangle$	3.05 ±0.02	3.11 ±0.02
$\delta N_\pm$	1.35 ±0.01	1.29 ±0.01

TABLE III. $\bar{p}d$ cross sections in mb.

P_{Lab} (MeV/c)	Total	$(\bar{p}p)_D$ annihilation	$(\bar{p}n)_D$ annihilation	"Elastic"	$(\bar{p}n)_D$ annihilation $P_s \lesssim 100$ MeV/c
270.0	466.9±25.5	215.5±17.1	152.7±14.4	98.7±12.4	75.7±10.2
290.0	455.2±22.6	174.2±13.7	137.7±12.2	143.3±13.3	66.6± 8.5
310.0	459.0±20.1	161.0±11.8	139.9±11.0	158.1±12.4	76.8± 8.1
327.5	415.3±16.5	137.2± 9.4	121.9± 8.9	156.2±10.7	70.4± 6.7
342.5	424.5±15.8	145.3± 8.9	122.4± 8.2	156.8± 9.9	61.2± 5.8
357.5	372.1±13.7	126.3± 7.7	96.0± 6.7	149.8± 8.8	52.0± 4.9
372.5	368.4±12.6	120.8± 7.0	107.1± 6.6	140.5± 8.0	61.0± 5.0
387.5	356.3±11.1	121.1± 6.5	88.9± 5.6	146.3± 7.6	43.4± 3.9
402.5	357.4±10.8	116.3± 6.0	98.9± 5.5	142.2± 7.1	48.9± 3.9
415.0	341.9±12.5	122.0± 7.2	88.9± 6.1	131.0± 8.0	42.2± 4.2
425.0	300.7±11.5	105.2± 6.7	84.5± 6.0	111.0± 7.4	43.5± 4.3
435.0	281.3±17.4	90.5± 9.5	79.5± 8.9	111.3±11.3	43.3± 6.6
445.0	301.6±17.2	90.7± 9.1	88.8± 9.0	122.1±11.3	43.0± 6.3
455.0	309.1±16.3	103.9± 9.3	83.9± 8.4	121.3±10.7	44.9± 6.1
465.0	322.2±16.0	108.7± 9.1	92.1± 8.3	121.4±10.3	48.3± 6.0

Table II). The Γ_0 is substantially larger than Γ_1 and this rules out any theories of the annihilation completely degenerate in I-spin.

(b) The $\bar{p}d$ cross-section measurements are presented in Tables III and IV, while in Figs. 10 and 11, they are compared with all other published data. The data binning is compatible with the momentum resolution which varies from ±0.010 GeV/c at 0.45 GeV/c to ±0.025 GeV/c at 0.3 GeV/c. The "elastic" (interactions with outgoing antiprotons) cross section has been corrected for forward scanning losses. This correction was determined by extrapolating the t distribution (Fig. 12) to $t=0$; it was found to be energy independent, within errors, and equal to (14.3±0.7)%. (There was no difference in this fraction for momenta < 0.375 GeV/c and > 0.375 GeV/c.) Our measurements are in good agreement, within errors, with other bubble-chamber measurements[11,12] except for a point (Ref. 11) at ~0.44 GeV/c (Fig. 10) due to four-prong events (Fig. 11). They also [(Fig. 10(a)] overlap reasonably well with the high-statistics data of Ref. 2 with a discrepancy of ~2.5σ at 0.38 and 0.4 GeV/c possibly related to inherent difficulties in the transmission technique used in Ref. 2 (1 ft of D_2 target, thick transmission counters).

The total cross section [Fig. 10(a)] compared with

$$\sigma^T_{\bar{p}d}\,(mb) = 129 + 78/[P(\mathrm{GeV}/c)] \qquad (2)$$

an empirical relation[1,2] which fits the data well in the range of $\bar{p}$ momenta from ~(0.55–2.0) GeV/c. Our measurements show that the $\bar{p}d$ total cross section is substantially larger than expected,

TABLE IV. $\bar{p}d$ topological annihilation cross sections in mb. Only charged mesons are counted as prongs. Zero-prong events include charge exchange.

P (MeV/c)	Zero-prong events	One-prong events	Two-prong events	Three-prong events	Four-prong events	Five-prong events	Six-prong events
270.0	23.2±5.6	25.4±5.9	79.4±10.4	90.0±11.1	104.3±11.9	34.9±6.9	8.2±3.3
290.0	23.1±5.0	29.5±5.6	69.2± 8.7	78.7± 9.2	74.5± 9.0	28.5±5.5	6.5±2.6
310.0	14.4±3.5	24.2±4.6	58.7± 7.1	82.4± 8.4	82.1± 8.4	31.2±5.2	4.3±1.9
327.5	17.7±3.4	23.8±3.9	46.9± 5.5	69.1± 6.7	65.6± 6.5	27.2±4.2	5.8±1.9
242.5	22.4±3.5	21.3±3.4	49.3± 5.2	73.8± 6.4	68.5± 6.1	22.7±3.5	4.4±1.5
357.5	20.3±3.1	11.4±2.3	50.4± 4.9	56.9± 5.2	49.5± 4.8	24.9±3.4	5.2±1.6
372.5	17.6±2.7	21.4±2.9	39.6± 4.0	57.7± 4.8	56.1± 4.8	26.5±3.3	6.8±1.7
387.5	18.8±2.6	15.6±2.3	41.8± 3.8	56.4± 4.4	54.8± 4.4	14.8±2.3	4.5±1.3
402.5	15.4±2.2	17.7±2.3	47.8± 3.8	56.0± 4.1	48.3± 3.8	24.9±2.8	3.7±1.1
415.0	8.6±1.9	12.6±2.3	40.5± 4.1	55.0± 4.8	66.4± 5.3	19.4±2.9	5.5±1.5
425.0	12.5±2.3	15.7±2.6	38.0± 4.1	50.0± 4.7	45.0± 4.4	14.8±2.5	5.6±1.6
435.0	8.0±2.8	11.1±3.3	42.3± 6.5	55.3± 7.5	36.2± 6.0	12.1±3.5	4.0±2.0
445.0	11.9±3.3	17.4±4.0	37.5± 5.9	48.5± 6.7	38.5± 5.9	22.9±4.6	2.7±1.6
455.0	16.6±3.7	16.6±3.7	37.4± 5.6	51.5± 6.5	44.9± 6.1	15.8±3.6	5.0±2.0
465.0	18.1±3.2	13.6±3.2	32.5± 5.0	50.6± 6.2	49.8± 6.1	19.6±3.9	8.3±2.5

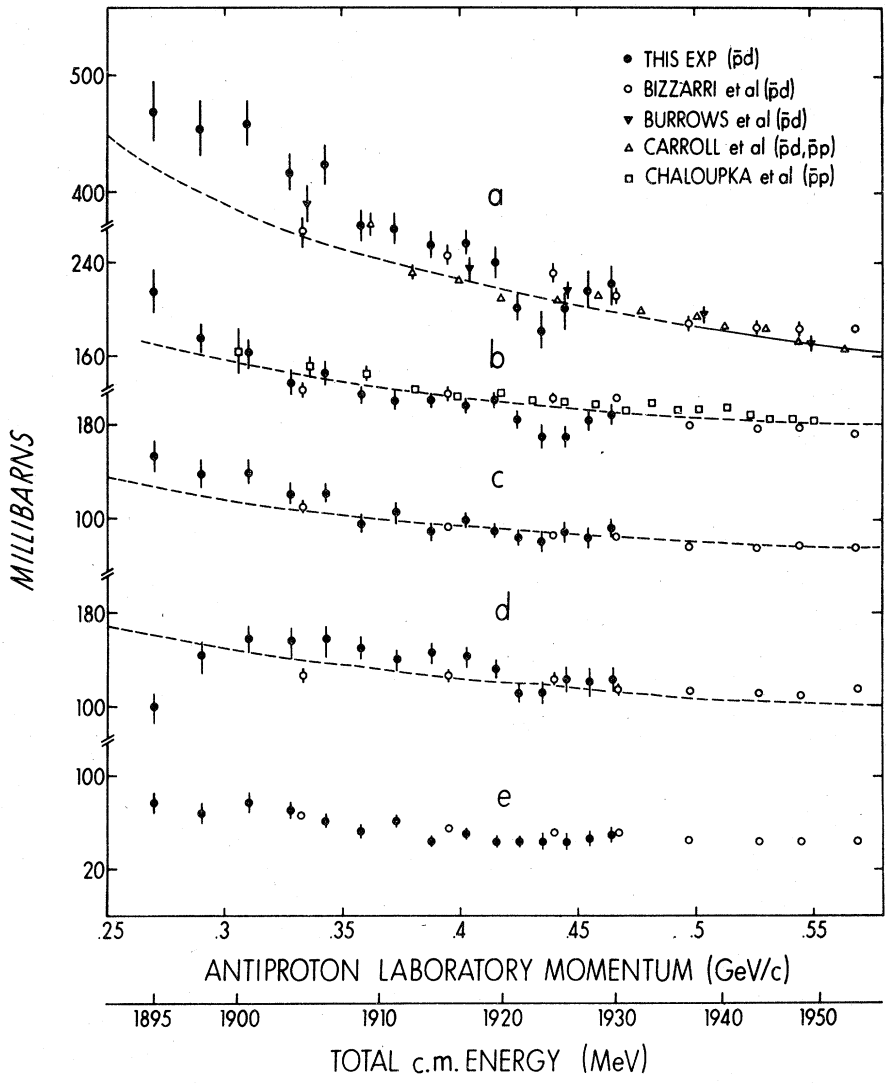

FIG. 10. $\bar{p}$ cross sections in deuterium: (a) total, (b) $\bar{p}p$ annihilation, (c) $\bar{p}n$ annihilation, (d) "elastic", (e) $\bar{p}n$ annihilation with invisible ($\lesssim$0.1 GeV/c) protons. Vertical broken scales are linear. See text for curves.

which suggests that new phenomena are contributing at energies below ~0.6 GeV/c. In Fig. 10(b) the $\bar{p}p$ annihilation cross sections as measured in H_2 and D_2 are presented. Except for the dip present in our data at ~0.43 GeV/c, there is no difference between hydrogen and deuterium, contrary to expectations for a smaller (~20%) cross section in D_2 due to shadow effects. This phenomenon was first noticed by Bizzarri *et al.*[11] It seems to us that this apparent absence of shadow effects can be understood if the $\bar{p}p$ annihilation cross section in D_2 is larger than in H_2 due to off-mass-shell effects. [Such an effect has been observed[3] in the production of the $\overline{N}N(1897)$.] The $\bar{p}p$ annihilation cross section fits well at higher energies[1] to the expression

$$\sigma_{\bar{p}p}^{\text{ann}}(\text{mb}) = 38 + 35/[P(\text{GeV}/c)] \,, \tag{3}$$

which seems to fit the H_2 and D_2 data [Fig. 10(b)] at low energies as well. In Fig. 10(c) the $\bar{p}n$ annihilation cross section is compared with Ref. 11 and

$$\sigma_{\bar{p}n}^{\text{ann}}(\text{mb}) = \left(\frac{\bar{p}n}{\bar{p}p}\right)_d \sigma_{\bar{p}p}^{\text{ann}} = 28 + 26/[P\ (\text{GeV}/c)] \tag{4}$$

using[13] $(\bar{p}n/\bar{p}p)_d = 0.75$ (see Table II). If $\bar{p}n$ in D_2 behaves similarly to $\bar{p}p$, then (4) is the $\bar{p}n$ (or $\bar{n}p$) annihilation cross section on free neutrons. Since the annihilation cross sections agree with the extrapolated cross sections from higher energies,

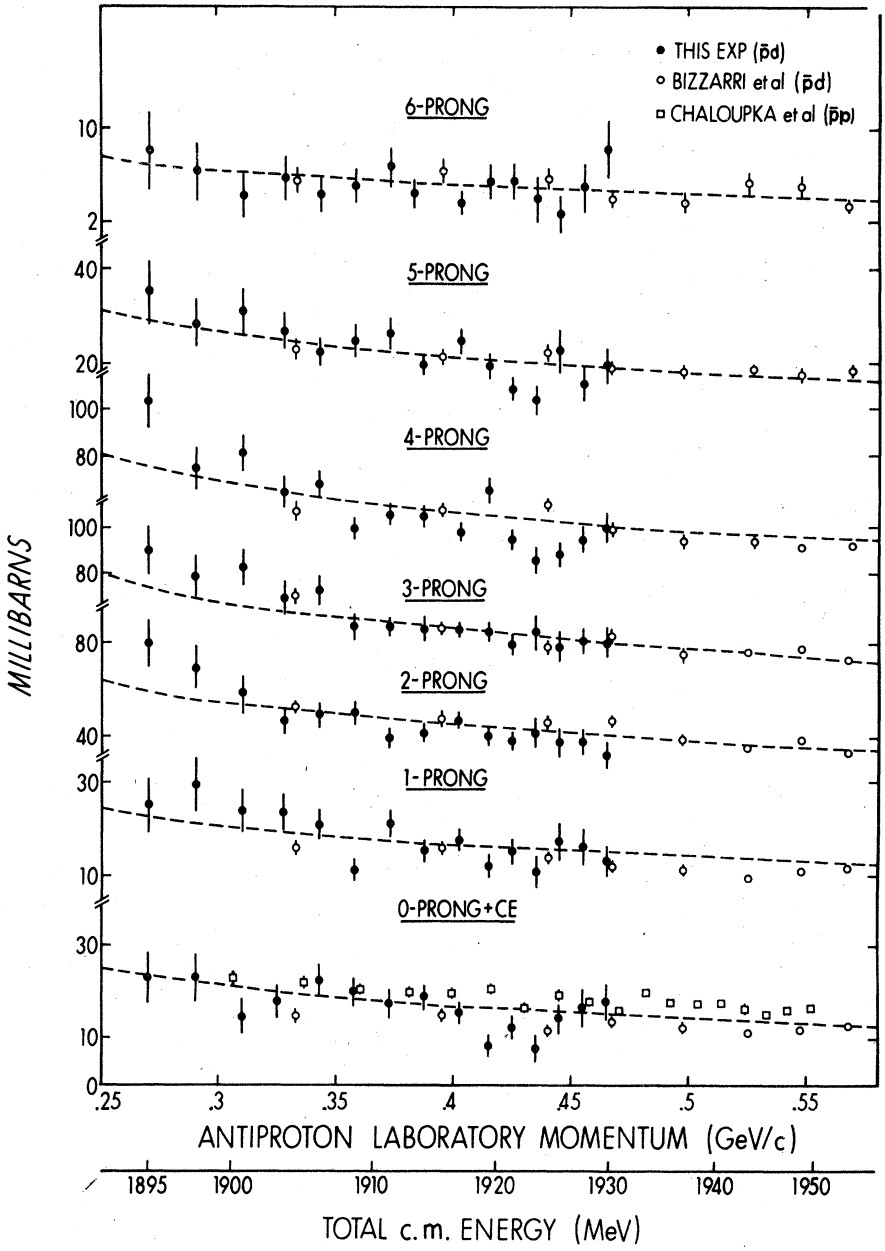

FIG. 11. Topological cross sections. Even-prong cross sections come from $\bar{p}p$ annihilations while the odd-prong ones come from $\bar{p}n$. Vertical broken scales are linear. See text for curves.

the deviation observed in the total cross section must be primarily due to the "elastic" ($\bar{p}d - \bar{p}d$, $-\bar{p}+p+n$) part. In Fig. 10(d) the "elastic" cross section is compared with

$$\sigma^{E}_{\bar{p}d}(mb) \equiv \sigma^{T}_{\bar{p}d} - \sigma^{\mathrm{ann}}_{\bar{p}p} - \sigma^{\mathrm{ann}}_{\bar{p}n}$$
$$= 63 + 77/[P\ (\mathrm{GeV}/c)]. \qquad (5)$$

Notice that the elastic cross section appears to be decreasing below 0.3 GeV/c. We have no reason to suspect that this decrease in instrumental. In Fig. 11 our topological cross sections are compared with other data[11,4] and with the relations (3) and (4) by multiplying them with the appropriate branching ratios (Table I).

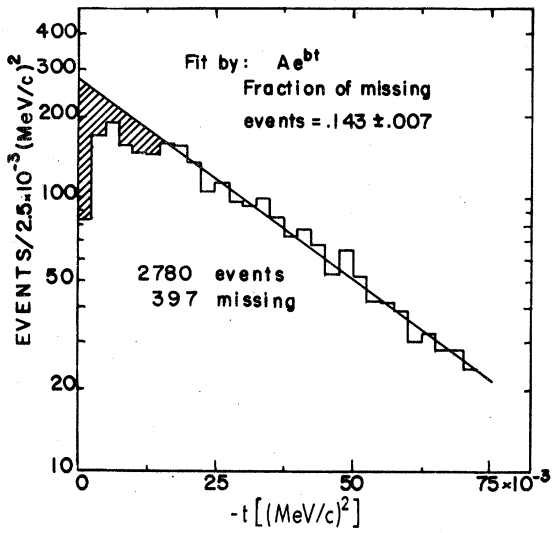

FIG. 12. t distribution of $\bar{p}d$ elastic-scattering events with or without deuteron breakup. $\bar{p}$'s going forward (small t) are missing.

IV. INTERPRETATION OF THE TOTAL CROSS SECTION

We shall now discuss an interpretation of the rising total cross section in terms of the $\bar{N}N(1897)$. The data shown in Fig. 13 and outside the S region have been fitted by averaging $\sigma_{\bar{p}\text{"}N\text{"}}$ in deuterium, namely

$$\sigma_{\bar{p}d} = \int d^3\vec{q}\,|\phi_d(\vec{q})|^2 \frac{2|\vec{k}|}{|\vec{p}|}\sigma_{\bar{p}\text{"}N\text{"}}, \tag{6}$$

assuming that the $\bar{p}$ interaction in deuterium are represented by the diagram in Fig. 14 where $\vec{p}$ is the $\bar{p}$ laboratory momentum, $\vec{q}$ the internal nucleon momentum, and $\vec{k}=(\vec{p}+\vec{q})/2$ the relative $\bar{p}$"N" momentum where the quotation marks refer to nucleons (bound) in deuterium. The $\bar{p}$"N" off-mass-shell cross section has been parametrized as follows:

$$\sigma_{\bar{p}\text{"}N\text{"}} = \sigma_0\left(1+\frac{f_B}{k}+\frac{f_R}{k^2}\frac{\Gamma_e\Gamma}{(E-E_R)^2+(\Gamma/2)^2}\right). \tag{7}$$

The first two terms represent the behavior seen at higher energies, while the third one is a resonance term which will be identified as the $\bar{N}N(1897)$. Following Blatt and Weiskopf[14] we use

$$\Gamma_e = \gamma k v_l(kR_l),$$

$$\Gamma_{e'} = \gamma k' v_l(k'R_l),$$

$$\Gamma = \Gamma_{e'} + \Gamma_r.$$

v_l is the centrifugal-barrier function [$v_0=1$, $v_1=x^2/(1+x^2)$, $v_2=v^4/(9+3x^2+x^4)$], $k'=\sqrt{mQ}$ the relative momentum of the outgoing on-shell elastic channel, γ the reduced elastic width, and Γ_r the

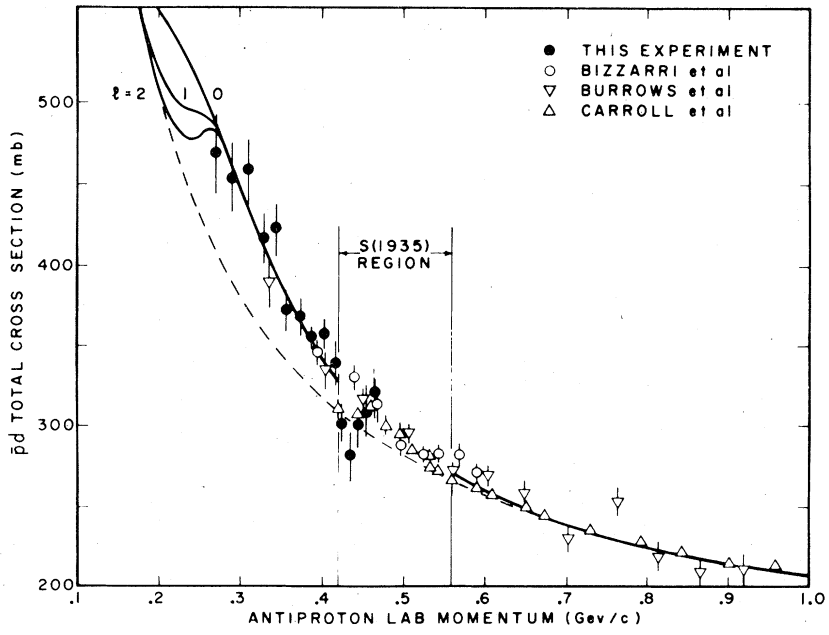

FIG. 13. $\bar{p}d$ total cross section at low momenta. Solid curves are the results of fits (see text for details) to $\sigma_0[1+f_B/k+f_R F_{BW,l}(1897)]$ as a function of l, while the dotted curve is the background $\sigma_0(1+f_B/k)$. The fits were made to the data shown outside the $S(1935)$ region. Notice that the lowest three points of Ref. 2 were excluded because of large momentum uncertainties.

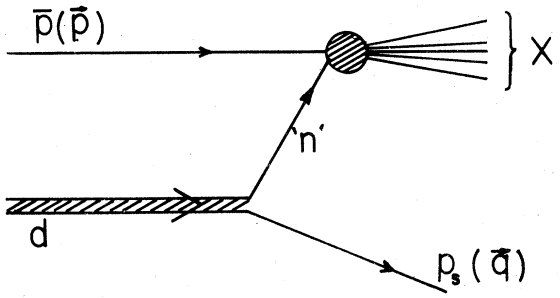

FIG. 14. The reaction $\bar{p}d \to (\bar{p}'n' \to X) + p_s$ in the impulse approximation. In the laboratory frame the off-mass-shell neutron "n" will have momentum $(-\vec{q})$.

inelastic total width. $Q = k^2/m - q^2/m$ is the center-of-mass $\bar{p}$"N" kinetic energy and R_l the radius of interaction for the l wave.

The $\bar{N}N(1897)$ was observed in $\bar{p}d \to p_s + (\bar{p}$"$n$"$)$ by measuring the $\bar{p}$"n" annihilation products via the missing-mass technique. Its production is very sensitive[3] to q, becoming maximum at ~0.250 GeV/c. This was interpreted[15] as a result of satisfying the condition $kR_l = [l(l+1)]^{1/2}$, or equivalently, $(mQ_R + q^2)R_l^2 = l(l+1)$ where $Q_R(\bar{N}N(1897)) \equiv 20$ MeV. Fits of the $\bar{p}d$ total cross section were made for $l = 0, 1, 2$ with R_l satisfying the above condition at $q = 0.25$ GeV/c. The results of these fits are shown in Table V and Fig. 13. The following conclusions may be drawn from this analysis :

(1) Equally good fits are obtained with $l = 0, 1, 2$ for the total cross section. Measurements at still lower energies, if our interpretation is correct, will be sensitive to the l values.

(2) Within the context of the potential $\bar{N}N$ model,[16] R_l favors $l = 1$. The fits with $l = 1, 2$ are consistent with the observed width (25 ± 6) MeV while $l = 0$ is excluded.

(3) The elasticity is large (Γ_r is small) and this independently confirms the observation made above that most of the deviation from $A + B/P$ behavior is due to the "elastic" part of the total cross section. This supports the baryonium picture for the $\bar{N}N(1897)$.

We were unable to reproduce the dip by adding interference terms between the $\bar{N}N(1897)$ and background and/or the $S(1935)$. One may therefore be tempted to discount the dip (~3σ) but in this case the evidence[2] for the $S(1935)$ in $\bar{p}d$ total cross section will be questionable. If, on the other hand, one takes the dip seriously, then a more complex nature (e.g., superposition of narrow states?) for the $\bar{N}N(1897)$ has to be assumed.[15]

V. COMPARISON WITH THE HAMILTON *et al.* DATA

Recently, new data on $\bar{p}d$ cross sections were reported[17] by a Berkeley-Brookhaven-Holyoke (BBH) collaboration in which the S meson is not seen in $\bar{p}p$, $\bar{p}d$ total and elastic cross sections as well as in $\bar{p}p$ backward elastic and charge exchange. We compare our measurements with those made by the BBH collaboration in Fig. 15.

Our total-cross-section measurements disagree with those of BBH. A least-square fit to our data gives $\sigma p = 126 + 30p$ (where σ is in mb and p is in GeV/c) showing a break at 0.54 GeV/c from the higher-energy behavior. Correspondingly, BBH gives $\sigma p = 71 + 132p$. Note that this break is about where the $S(1935)$ should start being produced. Our data would be consistent with an $S(1935)$ signature if the dip (~3σ) at ~0.43 GeV/c is real.

The differences in total cross section are not reconcilable since BBH state that their cross section is measured with an absolute normalization uncertainty of ±1.5%. The differences in the annihilation and elastic cross sections, however, may be reconcilable since BBH does not clearly distinguish between these cross sections. It seems to us, however, that the elastic cross section may be irreconcilable if only a normalization parameter is used. Our elastic scattering events extrapolate smoothly in the stopping region (Fig. 6) and we do not suspect any biases which would modify them in absolute value or in their energy dependence.

VI. SUMMARY AND CONCLUSIONS

We have measured the $\bar{p}d$ annihilation branching ratios at rest and in flight. As a function of charge multiplicity the at-rest and in-flight branching ratios fit very well to Gaussians. No significant variations are evident in these data as a function of energy. On the other hand, the $\bar{p}n/\bar{p}p$ ratios are significantly lower than unity which translates

TABLE V. Results of fits to the $\bar{p}d$ total cross sections (see text).

l	σ_0 (mb)	f_B (MeV/c)	$10^{-3} f_R$ (MeV^2/c^2)	Γ (MeV)	Γ_r (MeV)	R (fm) Fit	R (fm) Theory
0	132.1 ± 0.2	280.2 ± 0.2	7.1 ± 0.5	39^{+5}_{-3}	$0.004^{+5}_{-0.004}$		
1	132.0 ± 0.2	280.2 ± 0.2	11.4 ± 1	36^{+4}_{-2}	$1.8^{+3.5}_{-1.8}$	1.0 ± 0.1	1.10
2	131.8 ± 0.2	280.3 ± 0.2	20.5 ± 1.5	19^{+3}_{-2}	$2.2^{+3.4}_{-1.8}$	1.7 ± 0.1	0.75

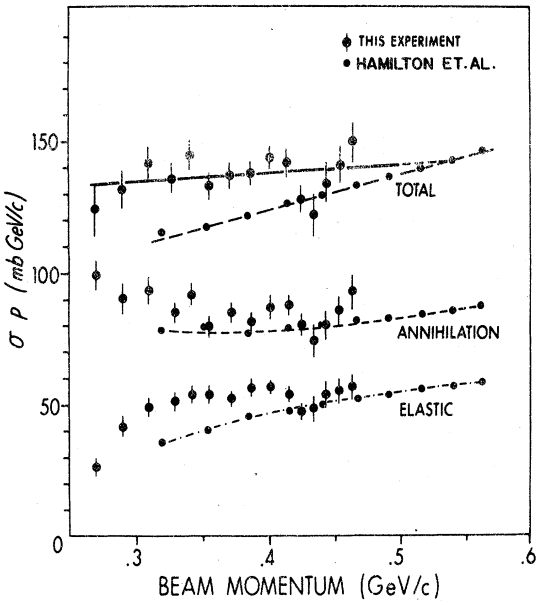

FIG. 15. Comparison of our $\bar{p}d$ cross sections with those of BBH collaboration. Discontinuous lines are eyeball fits to the BBH data. Continuous line is a least-square fit to our data points. The dashed lines in the total and annihilation cross sections are in agreement with the best fits obtained by Hamilton *et al.*[17]

into Γ_1/Γ_0 ratios of ~0.6–0.7.

The $\bar{p}p$ annihilation cross section in D_2 and H_2 are equal within errors. This is quite unexpected since shadow effects in deuterium at these low energies should have been large, ~20–30%, and therefore $\sigma_{\bar{p}p}^{ann}(H_2) > \sigma_{\bar{p}p}^{ann}(D_2)$. The statistical errors are typically ~5%. This could be viewed as a sign for dynamical effects which enhance the $\bar{p}p$ annihilation in D_2 due to off-mass-shell effects. Such a phenomenon was observed by us previously[3] in regard to the production of the $\bar{N}N(1897)$.

Our total $\bar{p}d$ cross section is in agreement with other bubble-chamber measurements[11,12] and reasonably overlap the Carroll *et al.*[2] data. They disagree, however, with recent measurements made by Hamilton *et al.*[17] They show a clear break in the $A+B/P$ behavior at ~0.54 GeV/c. This may be associated with the onset of the S-meson production. However, evidence for the production of the S meson in our data rests on a 3σ dip at ~0.43 GeV/c. If this dip is considered as a statistical fluctuation then there is no such evidence.

The deviation of the total cross section from the $A+B/P$ behavior has been fitted in magnitude and shape assuming $\bar{N}N(1897)$ production with parameters obtained from our earlier work.[3] The fits favor $l=1$ (on the basis of a reasonable radius of 1 fm) and a baryoniumlike (enhancement is mainly in the elastic channels) nature for the $\bar{N}N(1897)$. We would like to stress that this physical interpretation may not by any means be unique and other more complex interpretations could possibly account for the observed energy dependence of these cross sections. Clearly, much experimental and theoretical work remains to be done before the picture gets clarified in this interesting energy region of $\bar{N}N$ physics.

ACKNOWLEDGMENTS

This work was supported by the National Science Foundation, Washington, D. C. We are grateful to Soo-Yong Park, A. P. Balachandran, and C. Rosenzweig for several discussions.

[1]See, e.g., T. E. Kalogeropoulos, in *High Energy Physics and Nuclear Structure—1975*, proceedings of the Sixth International Conference, Santa Fe and Los Alamos, edited by D. E. Nagle *et al.* (American Institute of Physics, New York, 1975), p. 155.
[2]A. Carroll *et al.*, Phys. Rev. Lett. 32, 247 (1974).
[3]T. E. Kalogeropoulos and G. S. Tzanakos, Phys. Rev. Lett. 34, 1047 (1975).
[4]V. Chaloupka *et al.*, Phys. Lett. 61B, 487 (1976).
[5]W. Bruckner *et al.*, Phys. Lett. 67B, 222 (1977).
[6]I. S. Shapiro, Phys. Reports 35C, 129 (1978); C. B. Dover in *Proceedings of the Fourth International Symposium on NN Interactions, Syracuse, 1975*, edited by T. E. Kalogeropoulos and K. C. Wali (Syracuse Univ., Syracuse, 1975), Vol. II, Chap. VIII, pp. 37–91.
[7]See, e.g., G. F. Chew and C. Rosenzweig, Phys. Rev. D 12, 3907 (1975); Nucl. Phys. B104, 290 (1976); G. C. Rossi and G. Veneziano, Nucl. Phys. B123, 507 (1977); R. L. Jaffe, Phys. Rev. D 17, 1444 (1978).
[8]G. S. Tzanakos, Ph.D. dissertation, Syracuse University, 1976 (unpublished).
[9]C. Baltay *et al.*, Phys. Rev. 145, 1103 (1966).
[10]S. J. Orfanidis and V. Rittenberg, Nucl. Phys. B59, 570 (1973).
[11]R. Bizzarri *et al.*, Nuovo Cimento 22A, 225 (1974).
[12]R. D. Burrows *et al.*, Aust. J. Phys. 23, 819 (1970).
[13]We prefer to use the at-rest ratio because the in-flight ratio has a larger error due to the charge exchange uncertainties. At any rate, the use of either ratio is without any consequence to this paper.
[14]J. M. Blatt and V. F. Weisskopf, *Theoretical Nuclear Physics* (Wiley, New York, 1952), p. 420.
[15]T. E. Kalogeropoulos and G. S. Tzanakos, in *Antinucleon-Nucleon Interactions*, edited by G. Ekspong and S. Nilsson (Pergamon, New York, 1977).
[16]The theoretical radii (R_l) quoted in Table V were given to us by C. B. Dover.
[17]R. D. Tripp (private communcation). See also R. P. Hamilton *et al.*, Phys. Rev. Lett. 44, 1182 (1980).